communications earth & environment

ARTICLE

https://doi.org/10.1038/s43247-021-00218-3 OPEN

Ryugu's observed volatile loss did not arise from impact heating alone

Kosuke Kurosawa[1]✉, Ryota Moriwaki[2], Hikaru Yabuta[3], Ko Ishibashi[1], Goro Komatsu[4] & Takafumi Matsui[1,2]

Carbonaceous asteroids, including Ryugu and Bennu, which have been explored by the Hayabusa2 and OSIRIS-REx missions, were probably important carriers of volatiles to the inner Solar System. However, Ryugu has experienced significant volatile loss, possibly from hypervelocity impact heating. Here we present impact experiments at speeds comparable to those expected in the main asteroid belt (3.7 km s^{-1} and 5.8 km s^{-1}) and with analogue target materials. We find that loss of volatiles from the target material due to impacts is not sufficient to account for the observed volatile depletion of Ryugu. We propose that mutual collisions in the main asteroid belt are unlikely to be solely responsible for the loss of volatiles from Ryugu or its parent body. Instead, we suggest that additional processes, for example associated with the diversity in mechanisms and timing of their formation, are necessary to account for the variable volatile contents of carbonaceous asteroids.

[1] Planetary Exploration Research Center, Chiba Institute of Technology, Chiba, Japan. [2] Institute of Geo-Cosmology, Chiba Institute of Technology, Chiba, Japan. [3] Department of Earth and Planetary Systems Science, Graduate School of Science, Hiroshima University, Hiroshima, Japan. [4] International Research School of Planetary Sciences, Università d'Annunzio, Pescara, Italy. ✉email: Kosuke.kurosawa@perc.it-chiba.ac.jp

Carbonaceous (C-type) asteroids are considered the parent bodies of carbonaceous chondrite meteorites because of their similar reflectance spectra[1,2]. For example, a typical CI chondrite (e.g., Orgueil) contains 19.9 wt.% water and 3.1 wt.% carbon[3]. Spectroscopic observations of asteroids show that the outer main asteroid belt consists mainly of C-type asteroids[4], which are considered to have been one of the major carriers of water and organic matter to the inner Solar System, including Earth[5]. Recently, two C-type asteroids, Ryugu and Bennu, were extensively investigated by Hayabusa2[6] and OSIRIS-Rex[7], respectively. The remote sensing observations revealed that Ryugu and Bennu have experienced numerous impacts at a variety of impact energies[8,9]. Ryugu appears to have lost a significant amount of its volatiles during its history as its surface only exhibits a weak OH absorption band at 2.72 μm[10]. In contrast, Bennu apparently did not experience such volatile loss[11]. Solar heating of Ryugu during its temporary orbital excursion near the Sun cannot explain its volatile depletion[12]. Two hypotheses have been proposed to explain the depletion in volatiles. The first is that the Ryugu parent body experienced global internal heating due to decay of short-lived radionuclides[8]. The second is that devolatilisation was due to catastrophic disruption of the Ryugu parent body[13]. Although other possibilities, such as inefficient aqueous alteration and heating due to multiple impacts, cannot be ruled out[8], the two aforementioned scenarios are the most realistic based on the remote sensing data and our current knowledge of meteorites and asteroids[8,13].

In this study, we address the feasibility of the impact scenario, which is one of the leading hypotheses to explain the "dry" nature of Ryugu and the difference between Ryugu and Bennu. Thus, if the shock response of C-type asteroids is accurately understood, then it may be possible to constrain the origins of Ryugu and Bennu. Previous impact experiments using metal plates flying at <2 km s^{-1} [14–17], which is much slower than the typical impact velocity in the main belt region (4–5 km s^{-1} [18]), showed that chondritic meteorites could have easily lost their volatile content during hypervelocity impacts. This is the reason why impact heating has been considered as the cause of the diversity in the volatile contents of carbonaceous meteorites and those observed in the two asteroids.

The legacy results, however, seem to contradict a recent spectroscopic survey[19] that showed a widespread survival of hydrous minerals across the main belt region despite the intense impact bombardment throughout its history. In this study, we investigated shock-driven volatile loss to assess whether hypervelocity impacts can cause significant volatile loss from C-type asteroids. Two-stage light gas guns allow the shock response of materials to be robustly investigated, because they can accelerate a macroscopic (>1 mm) spherical projectile up to speeds of several km s^{-1} without heating of the projectile. However, chemical contamination from the gun operation has been a longstanding problem in such gas-gun experiments, including the 1980's experiments mentioned above. This has recently been overcome by the two-valve method[20]. In this study, we applied this experimental technique (Supplementary Note S1, Supplementary Table S1) to investigate the process of impact-driven volatile loss from carbonaceous chondrite-like materials (Supplementary Note S2, Supplementary Table S2), which are expected to be an analogue of C-type asteroid material.

Results

Laboratory experiments of impact-driven volatile loss from chondrite-like materials. We conducted hypervelocity impact experiments on a carbonaceous chondrite analogue with a mineral composition similar to the Orgueil meteorite[21] using a two-stage helium gas gun. The impact-generated gases were quantitatively measured with a quadrupole mass spectrometer (QMS), where the generated gas freely expands into a large free volume with respect to the volume of the shocked samples with volume ratios >10^{6-7}. In the experiments, Al_2O_3 projectiles were used that were accelerated to two different impact velocities of $v_{imp} = 3.7$ km s^{-1} (#459 and #461) and 5.8 km s^{-1} (#440, #447, and #448). Hereafter, we refer to the two velocities as "low v_{imp}" and "high v_{imp}", respectively. Figure 1 shows the temporal variations of the ion currents of selected masses for a high v_{imp} experiment (shot #448). The data supporting Fig. 1 can be found in Supplementary Data 1. The ion current for the mass number $M/Z = i$ is denoted as I_i. We confirmed that I_{40} (Ar^+) was stable during the measurement. A rise in I_4 (He^+), which is the gas that propels the projectile, was not detected, suggesting that chemical contamination was negligible. Abrupt increases in I_2 (H_2^+), I_{16} (CH_4^+), I_{28} (CO^+), I_{44} (CO_2^+), and I_{34} (H_2S^+) were detected. In contrast, we did not detect a sudden increase in I_{18} (H_2O^+), although our experimental system is capable of detecting impact-generated water vapour from hydrous minerals[20]. I_{18} did not spike immediately after the impact, but gradually increased with time. The time profile for I_{18} is different from the other species, suggesting that water vapour in micropores in the porous target was released due to the destruction of the target after the impact. For the other two shots at high v_{imp} (#440 and #447), the results are qualitatively the same as #448, although the peak values of I_i slightly differ. At low v_{imp} (#459 and #461), the peak I_i values for the species were several times lower than for the high v_{imp} experiments and a rise in I_{34} (H_2S^+) was not observed. We also conducted a series of calibration experiments (Supplementary Notes S3 and S4, Supplementary Figs. S1–S9, Supplementary Table S3). The contributions to the ion currents for lighter species from cracking of heavier species due to electron impacts in the QMS were investigated using standard gases. We determined such contributions to I_i from the raw signals by using the cracking patterns obtained for standard gases. This procedure is described in the Supplementary Note S4. We measured the amounts of the detected species quantitatively by integrating the time profiles of the ion currents and assuming the ratios of the integrated values to that of CO_2 were linearly proportional to the molar ratios to CO_2. We confirmed that this assumption is valid, at least for the molar ratio of CH_4 to CO_2, in the calibration experiments (Supplementary Note S3). Figure 2 shows the produced micromoles of H_2, CH_4, CO, CO_2, and H_2S. The main product was CO_2 in all shots. The mass of the CO_2 production corresponds to 0.2–0.3 and 1–2 wt.% of the projectile mass M_p at low and high v_{imp}, respectively. The amounts of the reducing species (H_2, CH_2, and CO) that were generated were 10–50 mol.% of the CO_2 produced. The amount of sulphur-bearing gases produced was only 0.01–0.1 mol.% of the carbon-bearing gases, although the

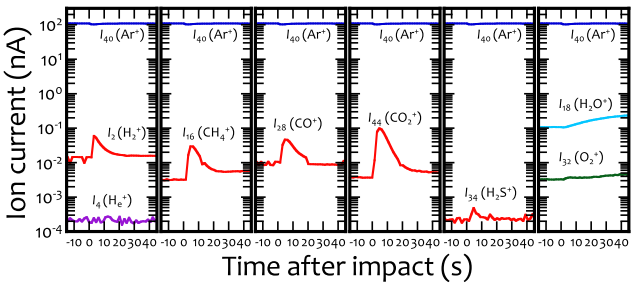

Fig. 1 Mass spectrometry data for the generated gas species. The graphs show the temporal variation of the ion currents for gases with the mass numbers I_i for shot #448 (high v_{imp}). The time variations for the ion counts can be found in Supplementary Data 1.

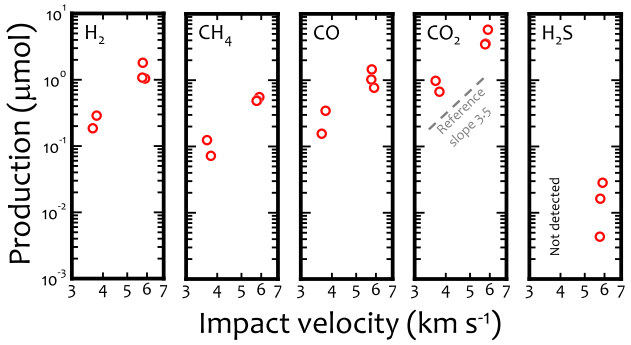

Fig. 2 Plots of the amounts of impact-produced species vs. impact velocity. Note that both the *x*- and *y*-axes are shown with a log scale. In the panel for CO_2, a reference slope that represents a power law with an exponent of 3.5 is also shown. The data supporting Fig. 2 are summarised in the Supplementary Table S2.

molar ratio of sulphur to carbon of the simulant is close to unity. We also found that water loss from hydrous minerals in the target (~50 wt.% of the carbonaceous chondrite analogue) was not significant. The upper bound of the released water vapour was estimated to be 7 wt.% of M_p (Supplementary Note S3, Supplementary Fig. S5). We confirmed that the chemical composition (e.g., CO/CO_2 and H_2/CO) of the generated species does not vary with v_{imp}. In contrast, the production of H_2, CH_4, CO, and CO_2 depends strongly on v_{imp} ($\propto v_{imp}^{3.5}$). We also conducted a control experiment with a basalt block, which is volatile-free, and confirmed that the detected species did indeed originate from the simulated CI meteorite target (Supplementary Note S5, Supplementary Figs. S10 and S11).

Discussion

Hypervelocity impacts in the main asteroid belt are not responsible for volatile loss. The pressures and temperatures experienced in the target were estimated with the iSALE-2D shock physics code[22–24] (Supplementary Notes S6 and S7, Supplementary Tables S4–S6). We used the ANalytical Equations Of State (ANOES)[25] to describe the thermodynamic response of a simplified model target composed of 25% porous serpentine. The residual (post-shock) temperatures of the heated material were derived from the simulations (i.e., the temperature after release from a state of high shock pressure). Note that this is in contract to the results reported in Michel et al. (2020)[13], in which peak-shock temperatures were considered. This allowed us to accurately estimate the role of impact heating on impact-induced devolatilisation.

We conducted two sets of numerical simulations called the Lab–simulation and Ryugu–simulation (see Methods). Figure 3 shows typical examples of the simulations, which plot the expected residual temperature after a pressure release T_{res} (Supplementary Note S8, Supplementary Fig. S12, Supplementary Table S7). The region highlighted in red indicates the heated region that experienced partial devolatilisation. Both simulations exhibit a similar thermal structure such that highly heated materials (T_{res} ~ 800 K where devolatilisation of the CI chondrite analogue initiates) are initially located within a distance of 1–2 D_p from the impact point and form a thin high-temperature layer beneath the crater floor. Devolatilisation can only occur from this layer. Figure 4 shows the cumulative mass as a function of peak pressure and entropy. The data supporting Fig. 4a and b can be found in Supplementary Data 2 and 3, respectively. The corresponding impact velocities required to produce a similar mass distribution in the case of a hypothesised catastrophic collision onto the parent body of Ryugu pertaining to low and high v_{imp} are estimated to be 4.0–4.5 and 6.0–7.0 km s^{-1}, respectively, in terms of both the peak pressure and expected residual temperature. Given that the most probable v_{imp} in the main asteroid belt region is estimated as 4.4 km/s[18], our impact experiments at low and high v_{imp} simulate typical and relatively high-speed collisions, respectively. It is worthwhile to mention here on the results by Tyburczy et al. (1986)[17]. They conducted shock recovery experiments on chips of the Murchison meteorite, and achieved relatively high pressures as shown in the Fig. 4a. They also detected volatile loss from the target. However, their experiment was conducted in a closed system where a sample was sealed in a stainless-steel container. Thus, the thermodynamic path experienced by the target was rather complex, and it is difficult to apply these results to natural impact events[26]. The details of the shock physics modelling are summarised in the Supplementary Notes S6 and S7.

Here we discuss the nature of impact devolatilisation of the simulated CI meteorite material. By detailed consideration of the volatile budget in the target material, energy partitioning during shock propagation, and the chemical composition of the generated gas (Supplementary Note S8, Supplementary Figs. S13–S16, Supplementary Table S8), we infer that the devolatilised volume is limited to only ~10% of the predicted value due to local energy concentration regardless of impact velocity. The temperature of the local hot region is estimated to be 1200–1650 K based on the measured CO/CO_2 molar ratio and oxygen fugacity assuming a CI composition[27]. The detected H_2, CO, and CO_2 are expected to have been produced by oxidation of the organics by water vapour and molecular oxygen derived from dehydration of Mg-serpentine and thermal breakdown of magnetite into wüstite and/or metallic iron in the vicinity of the local hot region. Mg-serpentine and magnetite are the first- and second-most abundant minerals in the CI meteorite analogue. The local hot region is likely to be produced by the shear velocities between different grains in the target, because of the large density contrast between the constituent minerals (1–5 Mg m^{-3}) (Supplementary Note S8, Supplementary Fig. S15). The released water vapour from the local hot region is estimated to be 1–2 wt% of the projectile mass (Supplementary Note S8, Supplementary Fig. S16). The temperature outside of the hot region would not have been high enough to cause oxidation of the organics. Outside the local hot region, only pure pyrolysis of the organics in the target occurred (700–800 K[21]). The measured CH_4 would have come from this region.

We now consider the effect of the impact obliquity on the total gas production. Although we performed vertical impact experiments in our laboratory, virtually all natural impacts occur at oblique incident angles to target bodies[28]. A previous hydrocode simulation[29], which did not consider any material strengths in their calculations, shows that the degree of shock heating decreased with the lowering impact angle measured from the target surface. In contrast, an oblique impact experiment[30] demonstrated that subsequent shear heating after shock propagation rather enhanced the total gas production during oblique impacts. A three-dimensional shock physics modelling[31] confirmed the role of the shear heating, but also showed that the degree of impact heating due to both shock and post-shock shear heating in oblique impacts of 45 degrees was similar to that pertaining to vertical impacts. Thus, it seems that the enhancement of shear heating during oblique impacts acts to compensate for the weaker shock heating during oblique impacts than vertical impacts. Consequently, we suggest that the total gas production obtained in this study would be a good approximation in the case of oblique impacts. Nevertheless, future experimental confirmation is required on this point.

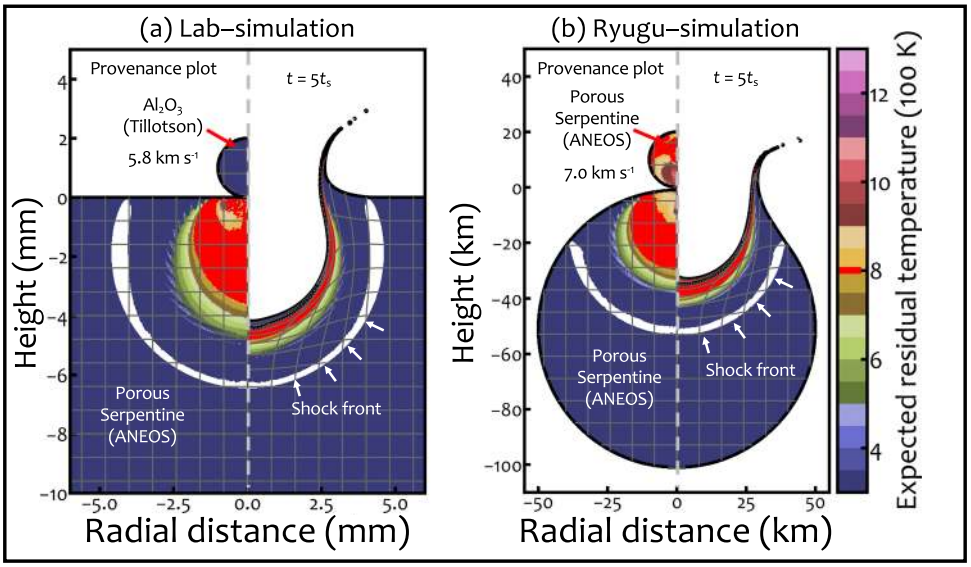

Fig. 3 Numerical results. a The result of the Lab-simulation at the high v_{imp} obtained with the iSALE shock physics code. A snap shot (right) and provenance plot (left) are shown. The colour indicates the expected residual temperature T_{res} calculated from the temporal entropy. A grid of tracer probes, plotted every 25 cells in the horizontal and vertical directions, is shown as grey lines. The location of the shock front is shown in a white line. Note that we did not calculate T_{res} in the Al_2O_3 projectile. **b** The same as (**a**), except the result of the Ryugu-simulation is shown. In this calculation, the impact velocity was set to 7 km s^{-1}. In these panels, the results are shown for $t = 5t_s$ (t is the time after impact), where $t_s = D_p/v_{imp}$ and is the characteristic time for projectile penetration, and D_p is the projectile diameter. This time was chosen because at this point the impact heating is finished.

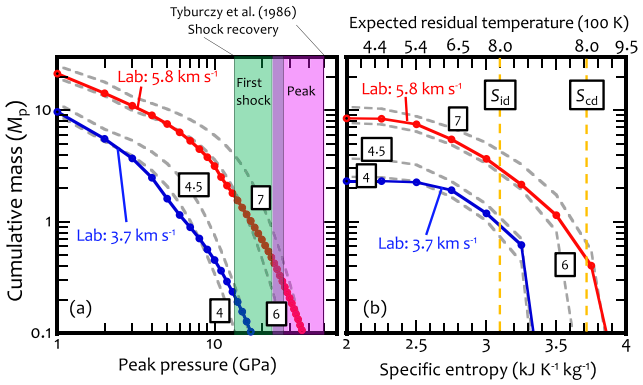

Fig. 4 Pressure and entropy (post-shock residual temperature) experienced during impacts. a The cumulative mass at a given peak pressure as a function of the peak pressure. The blue and red points correspond to the results of the Lab-simulation at low and high v_{imp}, respectively. The four dashed grey lines are the results of the Ryugu-simulation. The numbers in the black boxes on the lines are the impact velocities used in the Ryugu-simulation. The green and pink shaded regions indicate the range of pressures in a previous impact experiment[17]. **b** The same as (**a**), except the cumulative mass at a given entropy is shown as a function of entropy. The vertical dashed yellow lines indicates the entropies required for incipient and complete devolatilisation of the target (Supplementary Note S8). The expected residual temperature T_{res} is also shown on the top x-axis. The calculated results shown in Fig. 4a and b can be found in Supplementary Data 2 and 3, respectively.

Assuming that the simulated CI meteorite material is a suitable analogue of the constituent materials of C-type asteroids, our results predict the response of C-type asteroids to impact shocks as follows: (1) impact-induced volatile release, including water vapour and C-bearing species, is limited to only 2–4 wt.% of the impactor mass, even for a relatively high-speed collision in the main asteroid belt (6–7 km s^{-1}). This inefficient devolatilisation occurs because the devolatilised volume is limited by the local energy concentration due to frictional heating between the different grains; (2) devolatilisation of S-bearing minerals during a typical collision in the main asteroid belt is negligible, resulting in sulphur enrichment in the impactor footprint. Our results are consistent with two seemingly contradictory facts: the ubiquitous presence of hydrous minerals on C-type asteroids in the main belt[19] and non-negligible amounts of thermally metamorphosed (up to ~1000 K) CI/CM chondrites[32–34]. Consequently, the volatile depletion that is observed on the entire surface of Ryugu is unlikely to be due to a single catastrophic collision[13] or multiple impacts[8], at least at mutual collision velocities of up to 7 km s^{-1}, regardless of impactor density (Supplementary Note S9, Supplementary Fig. S17, Supplementary Tables S9 and S10). It should be mentioned here that we cannot rule out the possibility that massive volatile loss on Ryugu or its parent body was caused by extremely high-speed collisions (Supplementary Note S10, Supplementary Fig. S18) because an intensely heated volume experiencing complete devolatilization becomes a significant fraction at >7 km s^{-1}. Although such collisions are statistically rare (<15%)[18], impact devolatilization of carbonaceous asteroids during high-speed collisions at >7 km s^{-1} should be explored with future impact experiments in a fully open system. Finally, we propose that the bulk molar ratio of sulphur to carbon in returned samples may be a useful tracer of hypervelocity impacts onto Ryugu and Bennu and their parent bodies.

Methods

Impact experiments. The impact experiments were conducted using a two-stage light gas gun in the Hypervelocity Impact Facility of the Planetary Exploration Research Centre of the Chiba Institute of Technology (PERC/Chitech), Japan[35]. In this study, we focused on the shock responses of the constituent materials of C-type asteroids. However, C-type asteroid material is not yet available. In this study, C-type asteroid simulant provided by Exolith (https://sciences.ucf.edu/class/exolithlab/) was used as the target (Supplementary Note S2). We made pellets of this material with a hydraulic pump that were 54 mm in diameter and 30 mm thick. The bulk density of the pellets is 1.92 ± 0.03 Mg m^{-3}, which is close to the typical density of carbonaceous chondrites[36]. The target porosities were calculated with the dimensions and mass of the target pellets and a typical grain density (2.5 Mg m^{-3}) of carbonaceous chondrite meteorites[36]. Given that the shape of the pellets is cylindrical, we can easily measure the radius and length of the pellets and calculate the target volumes. The porosity was estimated to be 22–24%.

In order to investigate the devolatilisation behaviour of the target, we used the two-valve method developed in a previous study[20]. This method allows us to measure shock-generated gas in an open system, which has the same geometry as natural impacts and low levels of chemical contamination from the gun operation. In addition, we used helium gas instead of the normally used hydrogen gas for the projectile acceleration, in order to exclude hydrogen from the experimental chamber as this contributes to chemical reduction. A quadrupole mass spectrometer (QMS; Pfeiffer Vacuum Technology AG; Prisma plus QMG220) was used to analyse the shock-generated gas after each impact. An Al_2O_3 sphere that was 2 mm in diameter was used as the projectile, which was accelerated using a nylon slit sabot[37]. In this study, we conducted five shots (#440, #447, #448, #459, and #461) at two different impact velocities of $v_{imp} = 3.7$ km s^{-1} (#459 and #461) and 5.8 km s^{-1} (#440, #447, and #448) as described in the main text. Further details of the impact experiments, including the experimental procedures, the procedure of data reduction, and impact velocities achieved, are described in the Supplementary Note S1.

We also conducted a series of calibration experiments using a gas injection device and gas mixtures with different ratios of CO_2 to Ar, because CO_2 was the dominant gas detected after all the shots. A gas mixture of Ar and CO_2 was injected into the experimental chamber for a short duration (~0.1 s) using an automatic gate valve. Further details of the calibration are described in the Supplementary Note S3.

Numerical simulations. The ANalytical Equation Of State (ANEOS)[25] for serpentine[38] was used in the simulations. Serpentine is the main constituent of the simulated CI meteorite material and possibly of carbonaceous asteroids. The $\varepsilon-\alpha$ porosity compaction model[24] was also used to account for the porosity. We set the initial porosity to 25% to match the porosity of our target. This value is similar to that of carbonaceous chondrites[36].

The Tillotson equation of state[39] for Al_2O_3[40] was used for the projectile in the Lab–simulation that simulated the laboratory impact experiments. The impact velocity was set to be the same as that achieved in the experiments. Given that the projectile is denser (4.0 Mg m^{-3}) than the porous target (1.9 Mg m^{-3}), our laboratory impact experiments simulated impacts between two porous asteroids at a somewhat higher v_{imp} than the velocity achieved in the experiments, in terms of the experienced pressure and temperature in the target body.

In the Ryugu–simulation, we modelled vertical impacts of a spherical impactor with a diameter of 20 km onto a hypothetical Ryugu parent body with a 100 km diameter (Fig. 3b). Note that the size of the parent body is still debated. The calculation settings are similar to those used in a previous study[41], except that both the impactor and target were assumed to be porous serpentine with a porosity of 25%. The specific impact energy Q was varied from 1 to 400 kJ kg^{-1}, which is close to the range of the required energy densities between cratering and catastrophic disruption Q^* of 100-km-sized bodies[42,43]. The parameter sets and calculation settings are summarised in the Supplementary Notes S6 and S7. Our experimental results also help to predict the outcomes of impact events onto CI chondrites at any scale, although we considered a large-scale impact event in this study.

Data availability

The data supporting Figs. 1 and 4 can be available as Supplementary data available at https://zenodo.org/record/5055018#.YN239y33J4Q. The data supporting Fig. 2 is listed in Supplementary Table S3. The calculation results shown in Fig. 3 can be reproduced with the input parameters listed in Supplementary Table S4–S6.

Code availability

The iSALE shock physics code is not fully open-source, and it is distributed on a case-by-case basis to academic users in the impact community for non-commercial use only. A description of the application requirements can be found at the iSALE website (http://www.isale-code.de/redmine/projects/isale/wiki/Terms_of_use).

Received: 28 September 2020; Accepted: 1 July 2021;
Published online: 22 July 2021

References

1. Johnson, T. V. & Fanale, F. P. Optical properties of carbonaceous chondrites and their relationship to asteroids. *J. Geophys. Res.* **78**, 8507–8518 (1973).
2. Hiroi, T., Zolensky, M. E., Pieters, C. M. & Lipschutz, M. E. Thermal metamorphism of the C, G, B, and F asteroids seen from the 0.7 um, 3 um, and UV absorption strengths in comparison with carbonaceous chondrites. *Meteorit. Planet. Sci.* **31**, 321–327 (1996).
3. Baker, B. L. Review of organic matter in the Orgueil meteorite. *Space Life Sci.* **2**, 472–497 (1971).
4. Bus, J. S. & Binzel R. P. Phase II of the small main-belt asteroid spectroscopic survey: a feature based taxonomy. *Icarus* **158**, 146–177, (2002).
5. Hayatsu, R. & Anders, E. Organic compounds in meteorites and their origin. *Top Curr. Chem.* **99**, 1c–37c (1981).
6. Watanabe, S. et al. Hayabbusa2 arrives at the carbonaceous asteroid 162173 Ryugu—A spinning top-shaped rubble pile. *Science* **364**, 268–272 (2019).
7. Lauretta, D. S. et al. The unexpected surface of asteroid (101955) Bennu. *Nature* **568**, 55–60 (2019).
8. Sugita, S. et al. The geomorphology, color, and thermal properties of Ryugu: Implications for parent-body processes. *Science* **364**, eaaw0422 (2019).
9. Walsh, K. J. et al. Craters, boulders and regolith of (101955) Bennu indicative of an old and dynamic surface. *Nat. Geosci.* **12**, 242–246 (2019).
10. Kitazato, K. et al. The surface composition of asteroid 162173 Ryugu from Hayabusa2 near-infrared spectroscopy. *Science* **364**, 272–275 (2019).
11. Hamilton, V. E. et al. Evidence for widespread hydrated minerals on asteroid (101955) Bennu. *Nature Astronomy* **3**, 332–340 (2019).
12. Morota, T. et al. Sample collection from asteroid 162173 Ryugu by Hayabusa2: implications for surface evolution. *Science* **368**, 654–659 (2020).
13. Michel, P. et al. Collisional formation of top-shaped asteroids and implications for the origins of Ryugu and Bennu. *Nat. Commun.* **11**, 2655 (2020).
14. Boslough, M. B., Weldin, R. J., & Ahrens, T. J. Impact-induced water loss from serpentine, nontronite and kernite, Proc 11th Lunar Scie Conf., pp. 2145-2158, (1980).
15. Lange, M. A. & Ahrens, T. J. Impact-induced dehydration of serpentine and the evolution of planetary atmospheres. *Proc. 13th Lunar Planet. Sci. Conf., Part1, J. Geophys. Res.* **87**, A451–A456 (1982).
16. Lange, M. A., Lambert, P. & Ahrens, T. J. Shock effects on hydrous minerals and implications for carbonaceous meteorites. *Geochim. Cosmochim. Acta* **49**, 1715–1726 (1985).
17. Tyburczy, J. A., Frisch, B. & Ahrens, T. J. Shock-induced volatile loss from a carbonaceous chondrite: implications for planetary accretion. *Earth Planet. Sci. Lett.* **80**, 201–207 (1986).
18. Bottke, W. F., Nolan, M. C., Greenberg, R. & Kolvoord, R. A. Velocity distributions among colliding asteroids. *Icarus* **107**, 255–268 (1994).
19. Usui, F., Hasegawa, S., Ootsubo, T. & Onaka, T. AKARI/IRC near-infrared asteroid spectroscopic survey: AcuA-spec. *Publ. Astron. Soc. Japan* **71**, 1–41 (2019).
20. Kurosawa, K. et al. Shock vaporization/devolatilization of evaporitic minerals, halite and gypsum, in an open system investigated by a two-stage light gas gun. *Geophys. Res. Lett.* **46**, 7258–7267 (2019).
21. Britt, D. T. et al. Simulated asteroid materials based on carbonaceous chondrite mineralogies. *Meteoritics Planetary Sci.* **54**, 2067–2082 (2019).
22. Amsden, A., Ruppel, H. & C. Hirt. SALE: A simplified ALE computer program for fluid flow at all speeds. *Los Alamos National Laboratories Report*, LA-8095: p. 101 (1980).
23. Ivanov, B. A., Deniem, D. & Neukum, G. Implementation of dynamic strength models into 2-D hydrocodes: Applications for atmospheric breakup and impact cratering. *Int. J. Impact Eng.* **20**, 411–430 (1997).
24. Wünnemann, K., Collins, G. S. & Melosh, H. J. A strain-based porosity model for use in hydrocode simulations of impacts and implications for transient crater growth in porous targets. *Icarus* **180**, 514–527 (2006).
25. Thompson, S. L. & Lauson, H. S. Improvements in the Chart-D radiation hydrodynamic code III: Revised analytical equation of state, pp. *SC-RR-71 0714* pp. 119, Sandia Laboratories, Albuquerque, NM (1972).
26. Ivanov, B. A. & Deutsch, A. The phase diagram of CaCO3 in relation to shock compression and decompression. *Phys. Earth Planet. Inter.* **129**, 131–143 (2002).
27. Schaefer, L. & Fegley, B. Jr. Redox states of initial atmospheres outgassed on rocky planets and planetesimals. *Astrophys. J.* **843**, 120 (2017).
28. Shoemaker, E. M. Impact mechanics at Meteor Crater, Arizona. In B. M. Middlehurst, & G. P. Kuiper (Eds.), The solar system, (Vol. 4, pp. 301–336). Chicago, IL: University of Chicago Press, (1963).
29. Pierazzo, E. & Melosh, H. J. Melt production in oblique impacts. *Icarus* **145**, 252–261 (2000).
30. Schultz, P. H. Effect of impact angle on vaporization. *J. Geophys. Res.* **100**, 21117–21135 (1996).
31. Wakita, S., Genda, H., Kurosawa, K., & Davison, T. M. Enhancement of impact heating in pressure-strengthened rocks in oblique impacts. *Geophys. Res. Lett.* **46**, 13678–13686 (2019).
32. Yabuta, H., Alexander, C. M. O. 'D., Fogel, M. L., Kilcoyne, A. L. D. & Cody, G. D. A molecular and isotopic study of the macromolecular organic matter of the ungrouped C2 WIS 91600 and its relationship to Tagish Lake and PCA 91008. *Meteorit. Planet. Sci.* **45**, 1446–1460 (2010).
33. King, A. J., Solomon, J. R., Schofield, P. F. & Russell, S. S. Characterising the CI and CI-like carbonaceous chondrites using thermogravimetric analysis and infrared spectroscopy. *Earth, Planets Space* **67**, 198 (2015).
34. King, A. J., Schofield, P. F. & Russell, S. S. Thermal alteration of CM carbonaceous chondrites: Mineralogical changes and metamorphic temperatures. *Geochimica et Cosmochimica Acta* **298**, 167–190 (2021).

35. Kurosawa, K. et al. Dynamics of hypervelocity jetting during oblique impacts of spherical projectiles investigated via ultrafast imaging. *J. Geophys. Res. Planets* **120**, 1237–1251 (2015).
36. Ostrowski, D. & Bryson, K. The physical properties of meteorites. *Planet. Space Sci.* **165**, 148–178 (2019).
37. Kawai, N., Tsurui, K., Hasegawa, S. & Sato, E. Single microparticle launching method using two-stage light gas gun for simulating hypervelocity impacts of micrometeoroids and space debris. *Rev. Sci. Instrum.* **81**, 115105 (2010).
38. Brookshaw, L. An Equation of state for serpentine, *Tech. Rep., working paper series* SC-MC-9813 (Queensland: Faculty of Sciences, University of Southern Queensland) (1998).
39. Tillotson, J. H. Metallic equations of state for hypervelocity impact. *Technical Report GA-3216*, General Atomic Report (1962).
40. Kurosawa, K., Genda, H., Azuma, S. & Okazaki, K. The role of post-shock heating by plastic deformation during impact devolatilization of calcite ($CaCO_3$). *Geophys. Res. Lett.* **48**, e2020GL091130 (2021).
41. Wakita, S. & Genda, H. Fates of hydrous materials during planetesimal collisions. *Icarus* **328**, 58–68 (2019).
42. Jutzi, M., Michel, P., Benz, W. & Richardson, D. C. Fragment properties at the catastrophic disruption threshold: the effect of the parent body internal structure. *Icarus* **207**, 54–65 (2010).
43. Suetsugu, R., Tanaka, H., Kobayashi, H. & Genda, H. Collisional disruption of planetesimals in the gravity regime with iSALE code: Comparison with SPH code for purely hydrodynamic bodies. *Icarus* **314**, 121–132 (2018).

Acknowledgements

This work was supported by ISAS/JAXA as a collaborative program with the Hypervelocity Impact Facility. We appreciate Sunao Hasegawa and Takaya Okamoto for assistance with the development of our experimental system. We thank Dimitri Veras and Tom Davison for their helpful comments about English writing. We also thank the developers of iSALE, including G. Collins, K. Wünnemann, B. Ivanov, J. Melosh, D. Elbeshausen, and Tom Davison. We thank three referees for their careful reviews that helped greatly improve the manuscript, and the editor for handling the manuscript. A part of numerical computations was carried out on the general-purpose PC cluster at Centre for Computational Astrophysics, National Astronomical Observatory of Japan. K. K. is supported by JSPS KAKENHI grants JP17H01176, JP17H01175, JP17K18812, JP17H02990, JP18H04464, and JP19H00726, and by the Astrobiology Centre of the National Institute of Natural Sciences (Grants AB261014 and AB281026).

Author contributions

K.K. carried out the impact experiments, analyses, and numerical simulations, and wrote the initial draft of the manuscript. K.K., G.K., H.Y., and T.M. conceived the initial research idea and designed the impact experiments. R.M. and K.I. assisted with the impact experiments and the interpretation of the results. All the authors discussed the results and their implications.

Competing interests

The authors declare no competing interests.

Additional information

Supplementary information The online version contains supplementary material available at https://doi.org/10.1038/s43247-021-00218-3.

Correspondence and requests for materials should be addressed to K.K.

Peer review information *Communications Earth & Environment Materials* thanks Alexander Krot, Peter H. Schultz and the other, anonymous, reviewer(s) for their contribution to the peer review of this work. Primary Handling Editor: Joe Aslin. Peer reviewer reports are available.

Reprints and permission information is available at http://www.nature.com/reprints

Publisher's note Springer Nature remains neutral with regard to jurisdictional claims in published maps and institutional affiliations.